Agricultural and Forest Meteorology 233 (2017) 171–182

Contents lists available at ScienceDirect

Agricultural and Forest Meteorology

journal homepage: www.elsevier.com/locate/agrformet

Land surface phenology derived from normalized difference vegetation index (NDVI) at global FLUXNET sites

Chaoyang Wu[a,*], Dailiang Peng[b,*], Kamel Soudani[c], Lukas Siebicke[d], Christopher M. Gough[e], M. Altaf Arain[f], Gil Bohrer[g], Peter M. Lafleur[h], Matthias Peichl[i], Alemu Gonsamo[j], Shiguang Xu[k], Bin Fang[l], Quansheng Ge[a]

[a] Institute of Geographical Sciences and Natural Resources Research, Chinese Academy of Sciences, Beijing 100101, China
[b] Key Laboratory of Digital Earth, Institute of Remote Sensing and Digital Earth, Chinese Academy of Sciences, Beijing, 100101, China
[c] University of Paris-Sud, CNRS, AgroParisTech, Laboratoire Ecologie Systematique et Evolution, Faculty of Sciences of Orsay, France
[d] University of Goettingen, Faculty of Forest Sciences and Forest Ecology, Bioclimatology Department, Goettingen, Germany
[e] Department of Biology, Virginia Commonwealth University, Richmond, VA 23284-2012, USA
[f] School of Geography and Earth Sciences, McMaster University, Hamilton, Ontario, L8S 4K1, Canada
[g] Department of Civil, Environmental and Geodetic Engineering, The Ohio State University, Columbus, OH, USA
[h] Department of Geography, Trent University, Peterborough, Ontario, K9J 7B8, Canada
[i] Department of Forest Ecology and Management, Swedish University of Agricultural Sciences Umeå, 90183, Umeå, Sweden
[j] Department of Geography and Program in Planning, University of Toronto, 100 St. George St., Toronto, ON, M5S 3G3, Canada
[k] State Key Laboratory of Remote Sensing Science, Institute of Remote Sensing and Digital Earth, Chinese Academy of Sciences, Beijing, 100101, China
[l] Department of Earth & Environmental Engineering, Columbia University, 500 W 120th St., New York, NY 10027, USA

ARTICLE INFO

Article history:
Received 29 May 2016
Received in revised form
13 November 2016
Accepted 25 November 2016
Available online 29 November 2016

Keywords:
Phenology
SOS/EOS
Remote sensing
NDVI
MODIS
SPOT-VGT
Forest

ABSTRACT

Phenology is an important indicator of annual plant growth and is also widely incorporated in ecosystem models to simulate interannual variability of ecosystem productivity under climate change. A comprehensive understanding of the potentials of current algorithms to detect the start and end for growing season (SOS and EOS) from remote sensing is still lacking. This is particularly true when considering the diverse interactions between phenology and climate change among plant functional types as well as potential influences from different sensors. Using data from 60 flux tower sites (376 site-years in total) from the global FLUXNET database, we applied four algorithms to extract plant phenology from time series of normalized difference vegetation index (NDVI) from both MODIS and SPOT-VGT sensors. Results showed that NDVI-simulated phenology had overall low correlation ($R^2 < 0.30$) with flux-derived SOS/EOS observations, but this predictive strength substantially varied by fitting algorithm, sensor and plant functional type. Different fitting algorithms can produce significantly different phenological estimates, but this difference can also be influenced by sensor type. SPOT-VGT simulated better EOS but no difference in the accuracy of SOS was found with different sensors. It may be due to increased frequency of data sampling (10 days for SPOT-VGT vs. 16 days for MODIS) during spring season when rapid plant growth does not help SPOT-VGT more sensitive to growth. In contrast, more frequent data acquisition favors better modeling of plant growth in autumn when a gradual decrease in photosynthesis occurs. Our study results highlight that none of these algorithm can provide consistent good accuracy in modeling SOS and EOS with respect to both plant functional types and sensors. More importantly, a rigorous validation of phenology modeling against ground data is necessary before applying these algorithms at regional or global scales and consequently previous conclusions on regional SOS/EOS trends should be viewed with caution if independent validation is lacking.

1. Introduction

Phenology is one of the most important variables controlling the interannual variability of both gross primary productivity (GPP) and net ecosystem productivity (NEP) (Richardson et al., 2010;

* Corresponding authors.
E-mail addresses: wucy@igsnrr.ac.cn (C. Wu), pengdl@radi.ac.cn (D. Peng).

http://dx.doi.org/10.1016/j.agrformet.2016.11.193
0168-1923/

Wu et al., 2013; Richardson et al., 2013; Fu et al., 2015). Accurate estimation of phenology across plant functional types globally has become an urgently needed task for a better understanding of carbon exchange in the backdrop of ongoing climate change, especially because poor interpretation of phenology leads inaccurate estimates of plant productivity and carbon sequestration (Baldocchi et al., 2001; Morisette et al., 2009; White et al., 2009; Richardson et al., 2012; Keenan et al., 2014a,b; Wu et al., 2016).

Remote sensing techniques offer a robust approach to tracking canopy phenology from space, with land surface phenology (LSP) examining the timing of recurring seasonal variation in vegetated land surfaces from synoptic sensors (de Beurs and Henebry, 2004; Friedl et al., 2006, 2010; Motohka et al., 2010; Jeong et al., 2011; Piao et al., 2011; Zhang et al., 2003; Zhang, 2015; Piao et al., 2015). Spatial and temporal variation in regional to global scale LSP transitions, such as the start and end of the growing season (SOS and EOS, respectively), has been successfully analyzed from satellite data, and coupled with drivers of such phenological changes (e.g., temperature, precipitation, radiation) (Gonsamo et al., 2012; Fu et al., 2014; Jeganathan et al., 2014; Melaas et al., 2013; Keenan et al., 2014a,b; Christian et al., 2015; Xu et al., 2015; Park et al., 2015; Forkel et al., 2015; Shen et al., 2015; Wu et al., 2016).

Phenological transitions (i.e., SOS and EOS) can be identified from seasonal dynamics via spectral vegetation indices such as the normalized difference vegetation index (NDVI, Rouse et al., 1974) and the enhanced vegetation index (EVI, Huete et al., 2002). While field measured NDVI have shown the potential of modeling phenology (Nagai et al., 2010a; Nagai et al., 2014), satellite observations (e.g., an NDVI threshold of 0.45) are also useful for landscape phenology monitoring of vegetation ecosystems in eastern US (Jenkins et al., 2002). Similarly, NDVI of 0.35 was used to model SOS of terrestrial ecosystems in China (Piao et al., 2006). Alternative approaches proposed to better represent the different NDVI ranges across plant functional types (e.g., half way between the minimum and maximum NDVI, White and Nemani, 2006) by selecting a locally tuned threshold (White et al., 2009), rather than a globally fixed one. Compared with threshold methods, the more widely used approach to extract SOS and EOS from the inflection or transition points identified in the time-series of remote sensing observations. Typically for these approaches, some form of a logistic regression model is fitted to the time series of a smoothed vegetation index and the transition point is identified as an inflection point in the fitted curve (e.g., Zhang et al., 2003; Garrity et al., 2011). NDVI and EVI are two frequently adopted vegetation indices for the estimation of SOS and EOS from various sensors of ground/satellite platforms. For example, these sensors typically included the advanced very high resolution radiameter (AVHRR) (Piao et al., 2006, 2011; Zhang et al., 2014), the moderate-resolution imaging spectroradiometer (MODIS) (Zhang and Goldberg, 2011; Wu et al., 2014), the SPOT-VGT data (Delbart et al., 2015; Wu et al., 2016), the medium resolution imaging spectrometer (MERIS) (Dash et al., 2010), the Hyperion imagery (Christian et al., 2015), the Landsat/TM data (Fisher and Mustard, 2007; Walker et al., 2012; Melaas et al., 2013), the digital repeat photography (Sonnentag et al., 2012; Keenan et al., 2014a,b; Klosterman et al., 2014; Melaas et al., 2016; Peichl et al., 2015), and other ground-based sensors and observation networks (Soudani et al., 2012; Hmimina et al., 2013; Ryu et al., 2014).

Although increasing efforts have been made to better estimate SOS/EOS from remote sensing, there are several outstanding uncertainties regarding the most robust way to model phenological transitions and, thereby, optimally drive ecosystem models (Richardson et al., 2012). First, as there are many different approaches to derive SOS and EOS from times series of vegetation indices, a comprehensive comparison among these approaches against ground-based observations is needed, and particularly comparing across various plant functional types (Garrity et al., 2011; Xin et al., 2015). The dynamic range and interannual variability of canopy greenness may limit the potential of one approach to a particular ecosystems, prohibiting its broader applicability (White and Nemani, 2006; Wu et al., 2014; Rodriguez-Galiano et al., 2015). Furthermore, most previous studies focused on single or multiple vegetation indices from one sensor alone, with few concurrently evaluating the potential of vegetation indexes from multiple sensors for phenological modeling. Here, we provided a comprehensive assessment of the performance of modeling LSP (SOS and EOS) with NDVI derived from two sensors (MODIS, and SPOT-VGT) and from four different fitting approaches, evaluated against data from 60 flux sites (376 site-years in total) in the global FLUXNET database, representing a wide range of plant functional types and ecosystems. Our goals are to answer the questions:

1) What is the potential of satellite-based NDVI in modeling SOS and EOS derived from flux measurements across plant functional types?
2) Do different fitting approaches make significant difference on the performance of NDVI as a predictor or phenological transitions?
3) How does this performance vary by sensor?

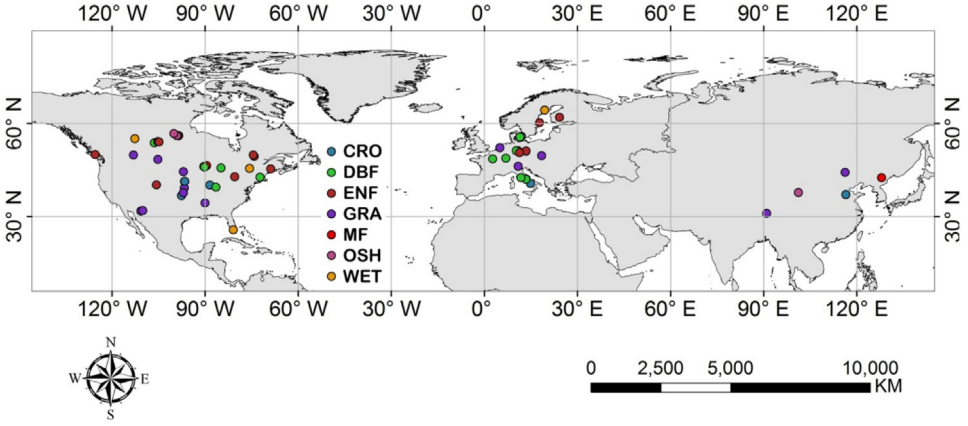

Fig. 1. Spatial descriptions of flux sites. CRO, DBF, ENF, GRA, MF, OSH and WET represent crop, deciduous broadleaf forest, evergreen needleleaf forest, grassland, mixed forest, open shrub and wetland sites, respectively (see supplementary Table S1 for details).

2. Methods

2.1. Flux sites

We used data from 60 flux sites of the FLUXNET database in this study, including 15 sites from Fluxnet-Canada (www.fluxnet-canada.ca), 5 sites in ChinaFlux (http://www.chinaflux.org/en/index/index.asp), 18 sites from European Eddy Fluxes databases cluster (www.europe-fluxdata.eu/newtcdc2/phome.aspx), and 22 sites from AmeriFlux (http://ameriflux.lbl.gov/) (Fig. 1). To reduce the probability of using poor quality data, certain rules were applied for site selection, including the availability and quality of data at each site as well as their spatial representativeness (e.g., less than 20% gap-filled in each year and no recent disturbances, i.e. fire, harvest). In total, 376 site-years of data were used with median of 6 years for each site. The vegetation at these sites was classified into seven plant functional types (PFT), with 17 evergreen needleleaf forest (ENF) sites (n = 112), 15 grassland (GRA) sites (n = 65), 4 wetlands (WET) sites (n = 23), 3 open shrub (OSH) sites (n = 12), 11 deciduous broadleaf forest (DBF) sites (n = 81), 3 mixed forest (MF) sites (n = 29), and 7 crop (CRO) sites (n = 54), respectively. Detailed description of each site is shown in supplementary Table S1.

2.2. NDVI from MODIS and SPOT-VGT

Time series of NDVI from both MODIS and SPOT-VGT were used. The global L3 vegetation indices (16-Day, 1 km, MOD13A2, Collection 6) were downloaded for each site (https://lpdaac.usgs.gov/dataset_discovery/modis/modis_products_table/mod13a2). Similarly, we also collected the SPOT-VGT NDVI data (10-Day, 1 km, S10) from the free VEGETATION Products Gateway (http://www.vito-eodata.be). The product has already been systematically corrected for the effects of atmosphere and topography (Maisongrande et al., 2004). For both products, NDVI of the central pixel at each flux location for each year was extracted following Wu et al. (2012). Selection of these two datasets were based on their data quality and comparable spatial resolutions.

2.3. Observed SOS and EOS from daily GPP

Continuous half-hourly CO_2 fluxes were measured at each site using the eddy-covariance technique (Baldocchi et al., 2001). For all sites, standard procedures (i.e., the artificial neural network (ANN) method (Papale and Valentini, 2003) and/or the marginal distribution sampling (MDS) method (Reichstein et al., 2005)) were applied to partition net ecosystem exchange (NEE) into gross primary productivity (GPP) and total ecosystem respiration (*Re*) (Papale and Valentini, 2003; Reichstein et al., 2005). Though different decomposition techniques may be used to flux data from various flux networks, almost all approaches give comparable results within 10% (Desai et al., 2008). Therefore, it is justified to use multiple sites in our analysis, which is also in line with other flux synthesis analyses reported on sites from global FLUXNET dataset (Wu et al., 2013; Verma et al., 2015).

Observed SOS and EOS from flux-measured GPP (i.e. carbon-flux phenology, Garrity et al., 2011) was used as the ground-based validation. A threshold of GPP (e.g., 1 g C m^{-2} d^{-1}) has been used to determine the phenological transitions in previous studies (Richardson et al., 2010; Dragoni and Rahman, 2012). However, a fixed GPP threshold may lead to a later SOS for ENF species and ecosystems with lower annual GPP, and a relative threshold (e.g., 10% of seasonal maximum) thus allows for variation in phenological events to be quantified and compared both inter-annually and spatially (Xin et al., 2015; Wu et al., 2013). Given these considerations, we used both fixed and relative threshold approaches to determine SOS and EOS from the daily GPP measurements and mean values were used as the ground observation data. Standard deviations for SOS and EOS between two methods were also calculated. We first used a negative exponential model, using polynomial regression and weights computed from the Gaussian density function to derive smoothed curves for daily GPP observations for each site. The SOS and EOS were then defined as the dates when smoothed curves of daily GPP first and last (for SOS and EOS, respectively) reached 1 g C m^{-2} d^{-1} and 10% (for fixed and relative threshold approaches, respectively) of the seasonal maximum GPP (Wu et al., 2012). An example is given to show the SOS and EOS determination approaches using daily GPP data at CA-OAS site for year 2008 (Fig. 2).

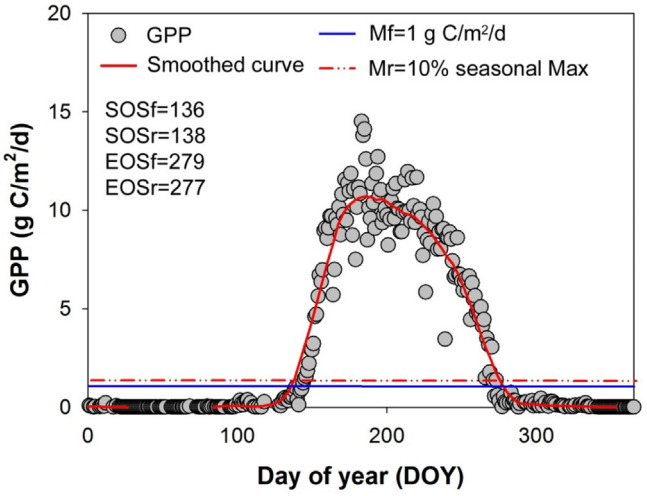

Fig. 2. Determination of the start and end of season (SOS and EOS) from daily gross primary productivity (GPP) data at CA-OAS in 2008. Mf and Mr represent SOS and EOS determined from fixed (i.e., GPP = 1 g C m^{-2} d^{-1}) and relative (i.e., GPP = 10% of seasonal maximum) thresholds, respectively.

2.4. SOS and EOS from NDVI data

Time series of NDVI was smoothed using the modified Savitzky-Golay (mSG) filter (Chen et al., 2004). The mSG filter is a simple but robust method based on the Savitzky-Golay (SG) filter (Chen et al., 2004), which employs vegetation index time-series characterizations to smooth out the noise caused by clouds or poor atmospheric conditions. According to Chen et al. (2004), the moving window was set to 4, and the quadratic function was used to fit the cure with an iteration time of 20. These smoothed NDVI time-series were linearly interpolated into daily time scale. We then used four approaches to determine SOS and EOS from time series of NDVI data based on previous studies (e.g., MODIS NDVI at CA-OAS in 2008, Fig. 3). The first method is the threshold approach (Fig. 3a). Unlike a globally fixed NDVI threshold (e.g., Piao et al., 2006), a locally tuned NDVI approach may have a better capability in modeling SOS and EOS (Kogan, 1997; White et al., 2009), and the $NDVI_{ratio}$ is calculated as

$$NDVI_{ratio} = (NDVI - NDVI_{min}) / (NDVI_{max} - NDVI_{min}) \quad (1)$$

where NDVI is the daily NDVI from either MODIS or SPOT-VEG. $NDVI_{max}$ and $NDVI_{min}$ are the seasonal maximum and minimum NDVI observations, respectively. SOS was determined when the $NDVI_{ratio}$ of 0.5 was reached in spring, and accordingly, the EOS was calculated when $NDVI_{ratio}$ declined to 0.5 in autumn (Fig. 3a).

We also used the simple logistic method proposed by Zhang et al. (2003) to determine SOS and EOS (Fig. 3b). The NDVI time series was first fitted as

$$NDVI_{f2}(t) = d + c/(1 + \exp(a + bt)) \quad (2)$$

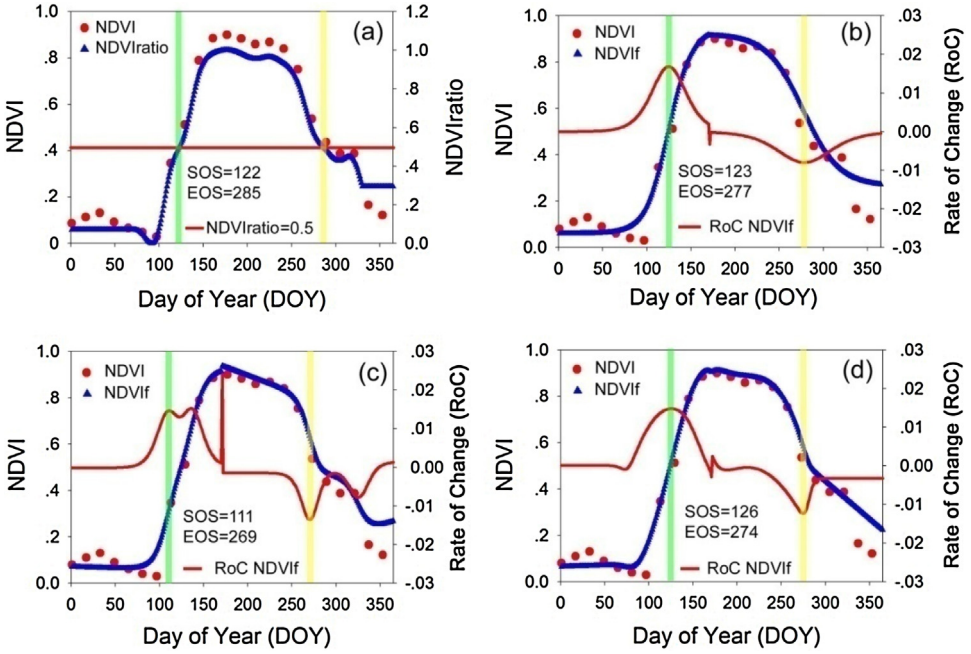

Fig. 3. An example of determination of start and end (SOS and EOS) using MODIS NDVI with the four fitting methods and a, b, c, d represent the four fitting methods, respectively (see Method section). NDVI and NDVIf in each subfigure are the observed NDVI and fitted NDVI. RoC NDVIf represents the rate of change (RoC) of the fitted NDVI curve. SOS and EOS for each method are indicated with vertical lines. Abrupt changes in RoC curves are caused by separate fitting of ascending and descending regions.

where $NDVI_{f2}(t)$ represents the simulated value of *NDVI* and time *t*. The whole time series is divided into ascending (spring) and descending (fall) sections by the maximum *NDVI* and each of the sections is fitted to the above function separately. *d* is the dormant seasonal baseline of greenness and *c* represents the amplitude of increase/decrease in greenness. *a* determines the timing of increase/decrease (in spring and fall, respectively) and *b* determines the rate of increase/decrease, (in spring and fall, respectively). The SOS and EOS are determined as the local extrema in the rate of change (RoC) of curvatures, respectively.

Though the simple logistic method has been extensively used in phenological studies (Hufkens et al., 2012; Zhang et al., 2003; Klosterman et al., 2014; Wu et al., 2016), it still has limitations in representing changes in greenness from extreme events such as summer drought or insect attack (Elmore et al., 2012; Wu et al., 2016). An improved algorithm was developed by Elmore et al. (2012), in which a new parameter (a_7) was included to simulate the summer decrease in canopy greenness (see Fig. 3c), and the double logistic function can be described as

$$NDVI_{f3}(t) = a_1 + (a_2 - a_7 t)\left[\frac{1}{1+\exp\left(\frac{a_3 - t}{a_4}\right)} - \frac{1}{1+\exp\left(\frac{a_5 - t}{a_6}\right)}\right] \quad (3)$$

Furthermore, we included the more generalized double logistic function formula which introduced two additional parameters (*q*

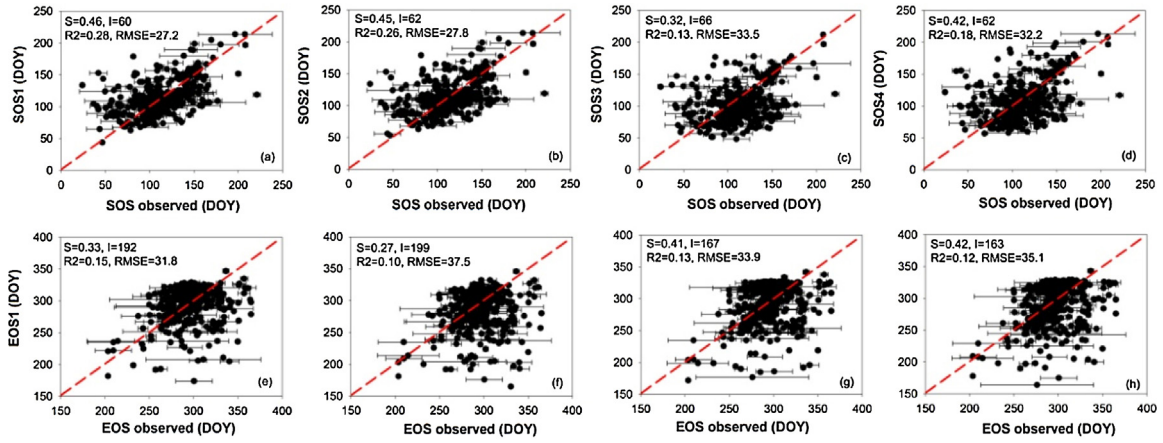

Fig. 4. Relationships between MODIS modeled start and end (SOS and EOS) of growing season and flux-based observations. The upper panels show the modeled SOS from the four methods (indicated by SOS1, SOS2, SOS3 and SOS4). The lower panels show the EOS from the four methods, respectively. Error bar indicates the standard deviation among the two flux-based observations (i.e., phenology from 1 g C m^{-2} d^{-1} and 10% of seasonal maximum). S and I are slope, and intercept of regression. Dash line represents 1:1.

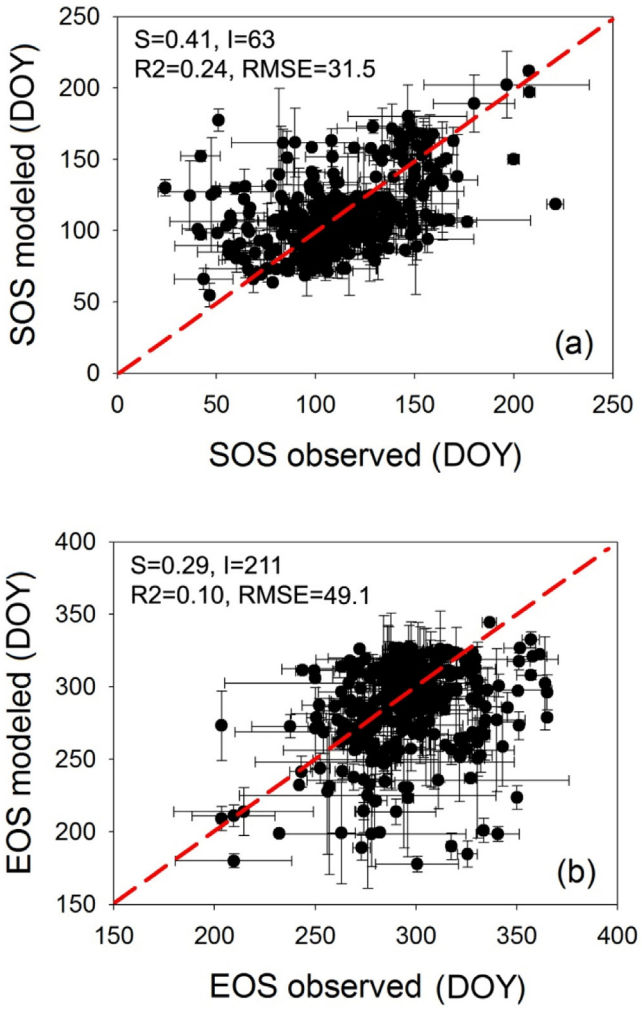

Fig. 5. Relationships between averages of MODIS derived (a) start and (b) end of growing season (SOS and EOS) from four approaches and observed phenology from flux sites. Error bar indicates the standard deviation. S and I are slope and intercept of regression. Dash line represents 1:1.

and v) to capture the different rates of increase near the lower and upper asymptotes (Klosterman et al., 2014) (see Fig. 3d).

$$NDVI_{f4}(t) = (a_1 t + b_1) + \left(a_2 t^2 + b_2 t + c\right) \left[\frac{1}{[1 + q_1 \exp(-h_1 (t - n_1))]^{v1}} - \frac{1}{[1 + q_2 \exp(-h_2 (t - n_2))]^{v2}}\right] \quad (4)$$

Separate ascending/descending fitted functions were used with all three methods, as well as the definitions of SOS and EOS. For each fitting, iterations were set to 2000 times until R^2 between the fitted curve and the smoothed curve reached 0.95, or did not change after 2500 times of iterations. Since four methods were used, the SOS and EOS for each method were referred as SOS_i and EOS_i, $i = 1$, 2, 3, 4. For example, SOS1, SOS2, SOS3 and SOS4 represent the SOS derived from the above four methods (Eqs. (1)–(4)) respectively.

2.5. Analysis approach

To compare the performances of different models in predicting SOS and EOS, we analyzed the correlations of the overall datasets (with functional groups combined) and for each plant functional type separately using the least-squares linear regression to calculate coefficients of determination (R^2) and p-value (significant level was set to a p-value of 0.05). The root mean square error (RMSE) was also used to evaluate the predictive strength of significant correlations. To better compare the model outputs for each fitting approaches, we used the analysis of variance (ANOVA) technique (Duncan's multiple range test, p=0.05) to analyze the differences among group means, since it can provide a statistical test of whether or not the means of several groups (both SOS and EOS) are equal, and therefore it generalizes the t-test to more than two groups.

3. Results

3.1. MODIS NDVI-modeled SOS and EOS

Modeled SOS and EOS derived from the four fitting methods were compared with flux-based observations (Fig. 4). All approaches produced significant ($p < 0.001$) relationships between SOS modeled and observations (Fig. 4a–d), though with relatively low R^2. SOS derived using the local threshold method (SOS1) showed the highest correlation with an R^2 of 0.28 ($p < 0.001$). Simple logistic (SOS2) had a comparable goodness-of-fit with an R^2 of 0.26 ($p < 0.001$). Predicted SOS from the double logistic (SOS3) only

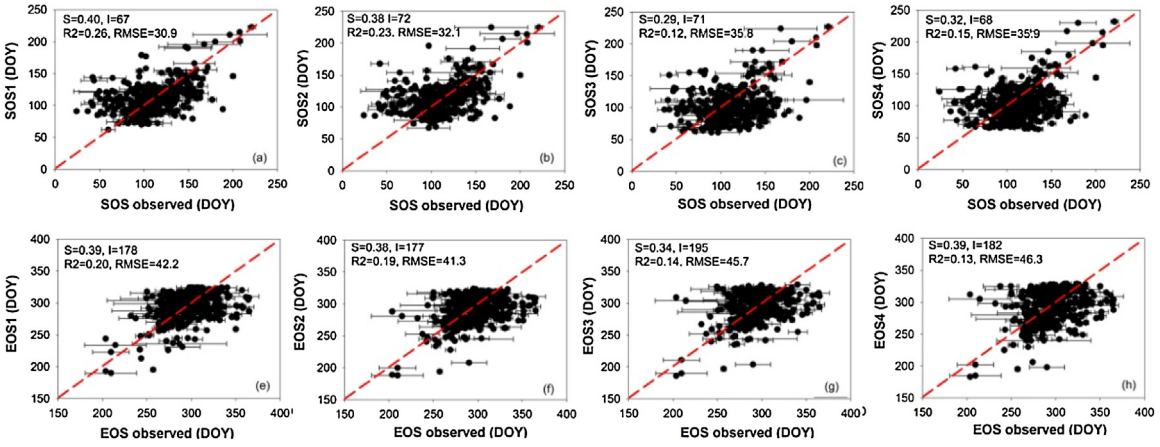

Fig. 6. Relationships between SPOT-VGT modeled start and end (SOS and EOS) of growing season and flux-based observations. The upper panels show the modeled SOS from the four methods (indicated by SOS1, SOS2, SOS3 and SOS4). The lower panels show the EOS from the four methods, respectively. Error bar indicates the standard deviation of two flux-based observations. S and I are slope and intercept of regression. Dash line represents 1:1.

explained 13% of observed variance and this percentage slightly increased to 18% for the generalized double logistic method (SOS4). For EOS, lower correlations ($R^2 < 0.15$) were found for all models compared with SOS (Fig. 4e-f). The local threshold method (EOS1) only explained 15% of in-situ variability while the R^2 for simple logistic, double logistic and general double logistic were 0.10 ($p < 0.001$), 0.13 ($p < 0.001$) and 0.12 ($p < 0.001$), respectively.

We also used the averages of four approaches to estimate SOS and EOS for all 60 flux sites (Fig. 5). We found that SOS estimates were significantly correlated with ground observations with R^2 of 0.24 ($p < 0.001$). The EOS, not surprisingly, was correlated with observed EOS with a lower R^2 of 0.11 ($p < 0.001$). It is notable that for overall data, model outputs tended to give earlier SOS compared with observations (i.e., bias of −2.4 days). Similarly, modeled EOS was also earlier than observations for all approaches.

3.2. SPOT-VGT NDVI modeled SOS and EOS

Using NDVI derived from SPOT-VGT data, we found that SOS modeled using the four approaches were all significantly correlated with observations for the overall dataset (also low correlation, $R^2 < 0.30$) combining all functional types, but differing in the degrees of correlation (e.g., different slopes, intercepts and RMSE for regressions) (Fig. 6). The local site data tuned threshold method predicted SOS that was best correlated with observed SOS ($R^2 = 0.26$, $p < 0.001$) and the double logistic method showed the lowest capability with R^2 of 0. 12 ($p < 0.001$). Similar results were also observed for EOS that the local tuned threshold method gave the best EOS estimates ($R^2 = 0.20$, $p < 0.001$). The simple logistic methods showed a comparable fit with an R^2 of 0.19 ($p < 0.001$). Surprisingly, the double logistic method and its general form only explained 14% and 13% of observed variations in EOS. When the mean derived from these four approaches was used, 21% of variations in SOS was explained by model output, and the percentage slightly decreased to 20% for EOS, as shown in Fig. 7.

3.3. Comparison across plant functional types

We also compared the MODIS-modeled SOS and EOS for each plant functional type (Figs. 8 and 9). Overall, substantial differences were found in the performance of these four methods in predicting SOS across the array of plant functional types included in our analysis. For example, none of the four methods provided reliable SOS estimates for ENF, WET, OSH and MF sites. In comparison, SOS for GRA sites were better modeled, with all approaches yielding SOS estimates that were significantly correlated with flux-based observations (R^2 between 0.30 and 0.42, $p < 0.001$). Similar results were also found for CRO sites with R^2 ranging from 0.14 ($p = 0.006$) for SOS3 and 0.45 ($p < 0.001$) for SOS1, respectively. For DBF sites, we found that observed SOS values were only significantly correlated with modeled SOS when calculated by the local threshold ($R^2 = 0.28$, $p < 0.001$) and simple logistic method ($R^2 = 0.25$, $p < 0.001$).

Compared with SOS, all models predicting observed EOS performed comparably for a given functional type (Fig. 9). No correlation was found between observed and modeled EOS for ENF, WET, OSH and MF sites, irrespective of methods. For DBF and CRO sites, all methods predicting EOS were significantly correlated with observations, though differing modestly in the strength of correlation. For example, R^2 ranged from 0.22 ($p < 0.001$) to 0.43 ($p < 0.001$) among the four modeling methods for DBF sites. For GRA sites, only modeled EOS from the simple logistic was not significantly correlated with observations, though R^2 for the other three methods were also low with R^2 from 0.12 ($p = 0.006$) for EOS1 to 0.20 for EOS4 ($p < 0.001$), respectively.

For each plant functional type, we also conducted the same analysis on SPOT-VGT modeled SOS/EOS and observed similar

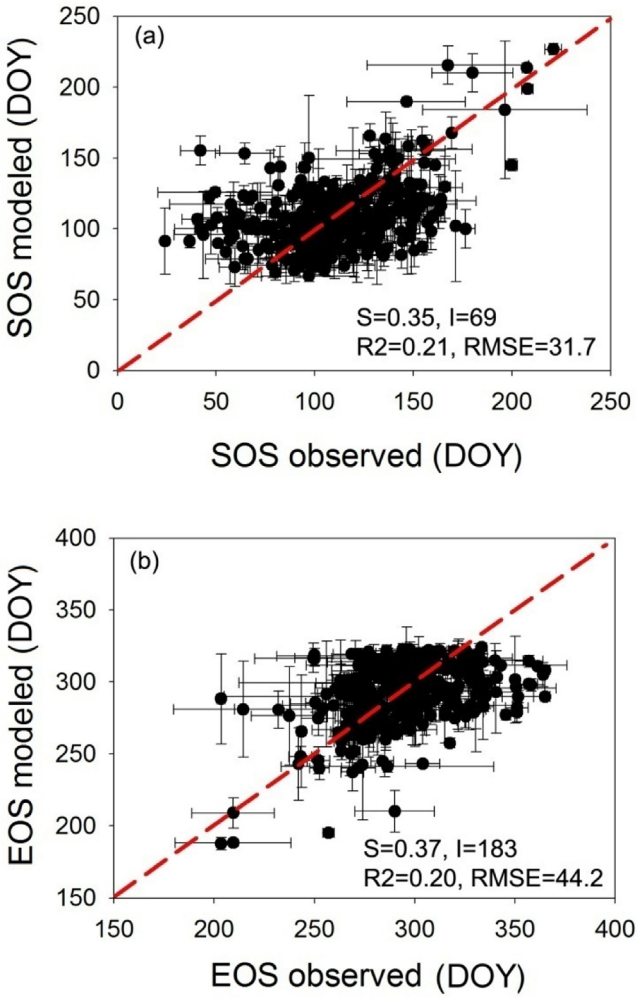

Fig. 7. Relationships between averages of SPOT-VGT derived (a) start and (b) end of growing season (SOS and EOS) from four approaches and observed phenology from flux sites. Error bar indicates the standard deviation. S and I are slope and intercept of regression. Dash line represents 1:1.

substantial differences in the predictive strength among the four modeling approaches both for SOS and EOS (Figs. 10 and 11). For example, neither SOS nor EOS observations from ENF, OSH and MF sites were significantly predicted from and of the four models. However, SOS estimated from all approaches was significantly correlated with observations for GRA sites with R^2 of 0.34 and 0.49 for SOS3 and SOS1, respectively. Comparable results were found for WET sites that only SOS1 was not significantly correlated with observed SOS. For DBF and CRO sites, both SOS1 and SOS2 were correlated with observations while the other two approaches can neither predict reliable SOS estimates. EOS for all species were not well modeled except that for CRO sites with significant correlations found for all approaches between model outputs and observations.

3.4. Comparison among predictive methods

The ANOVA analysis using Duncan's multiple range test showed that different modeling approaches may have significantly different predictive capabilities for different plant functional types. For MODIS-derived SOS, SOS1 was not significantly different from SOS2 for all plant functional types, which was also in line with SOS modeled from SPOT-VGT (Fig. 12a, c). MODIS predicted SOS from the double logistic method (i.e., SOS3) was significantly different from SOS1 and SOS2 for all plant functional types, which was also con-

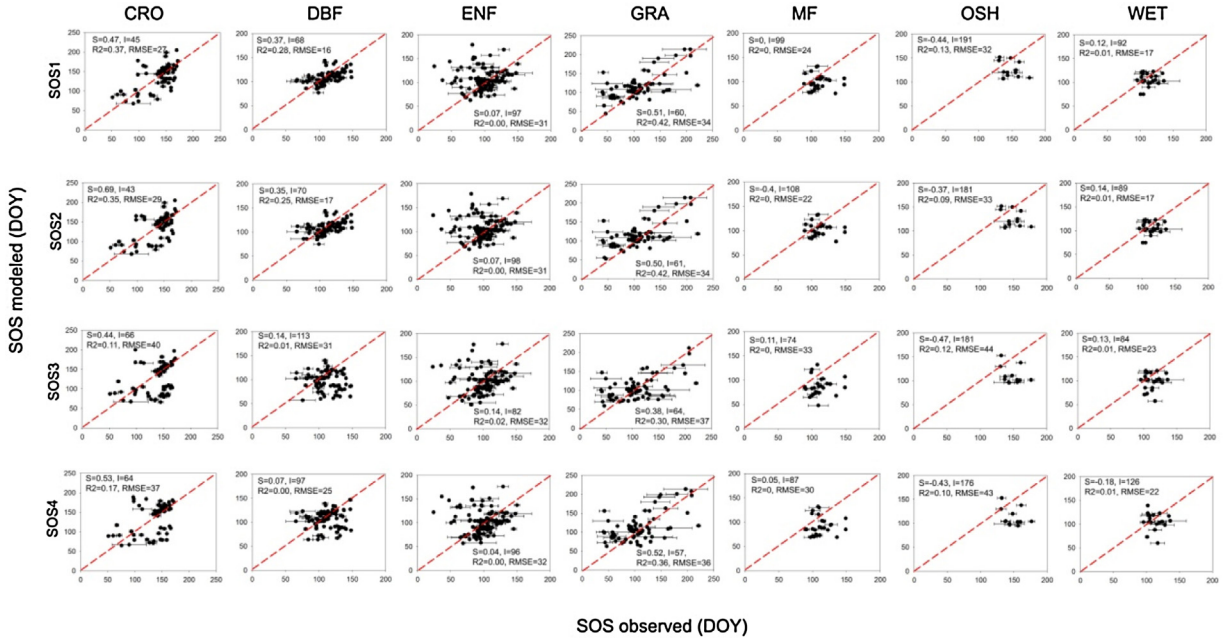

Fig. 8. Relationships between MODIS modeled start of growing season (SOS) and flux-based observations across plant functional types. SOS1, SOS2, SOS3 and SOS4 are model results for each data fitting approaches (see Method). CRO, DBF, ENF, GRA, MF, OSH and WET represent crop, deciduous broadleaf forest, evergreen needleleaf forest, grassland, mixed forest, open shrub and wetland sites, respectively. Error bar indicates the standard deviation of two flux-based observations. S and I are slope and intercept of regression. Dash line indicates 1:1.

sistently observed in the SPOT-VGT estimates (except for MF and CRO sites). No consistent result was found in the significance level between SOS3 and SOS4, either for MODIS or for SPOT-VGT. For EOS from MODIS, we found that EOS1 was significantly different from EOS2 except for OSH sites while it was opposite for SPOT-VGT estimates that for all plant functional types, EOS1 and EOS2 had the same significance level. No difference was observed between EOS3 and EOS4 for both sensors, except for OSH and CRO sites of SPOT-VGT estimates.

3.5. Comparison between sensors

We compared the averages (±s.d.) of model outputs (SOS and EOS) with flux-observations for each plant functional types from both sensors (Fig. 13). We found that for SOS, both MODIS and SPOT-VGT estimates were later than observations for ENF and GRA sites while earlier than observations for other plant functional types. For example, MODIS-modeled SOS were earlier than observations by 29 ± 8.6 and 16 ± 6.0 days for OSH and MF, respectively. This length

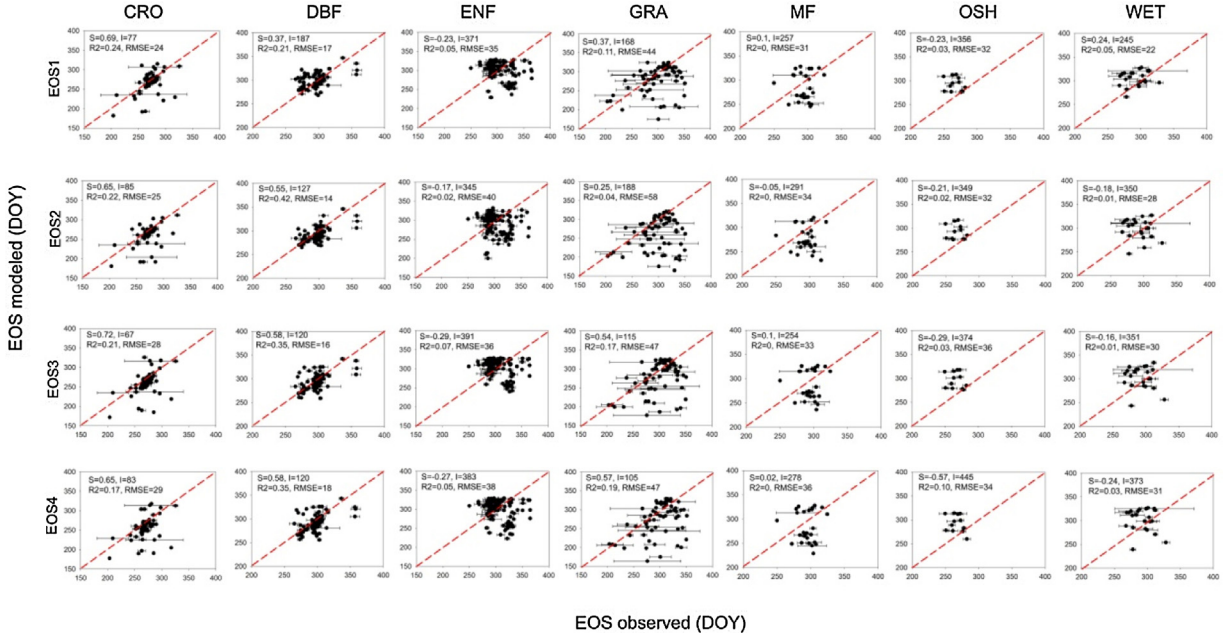

Fig. 9. Relationships between MODIS modeled end of growing season (EOS) and flux-based observations across plant functional types. EOS1, EOS2, EOS3 and EOS4 are model results for each data fitting approaches (see Method). CRO, DBF, ENF, GRA, MF, OSH and WET represent crop, deciduous broadleaf forest, evergreen needleleaf forest, grassland, mixed forest, open shrub and wetland sites, respectively. NS indicates that no significant correlation is observed. Error bar indicates the standard deviation of two flux-based observations. S and I are slope and intercept of regression. Dash line indicates 1:1.

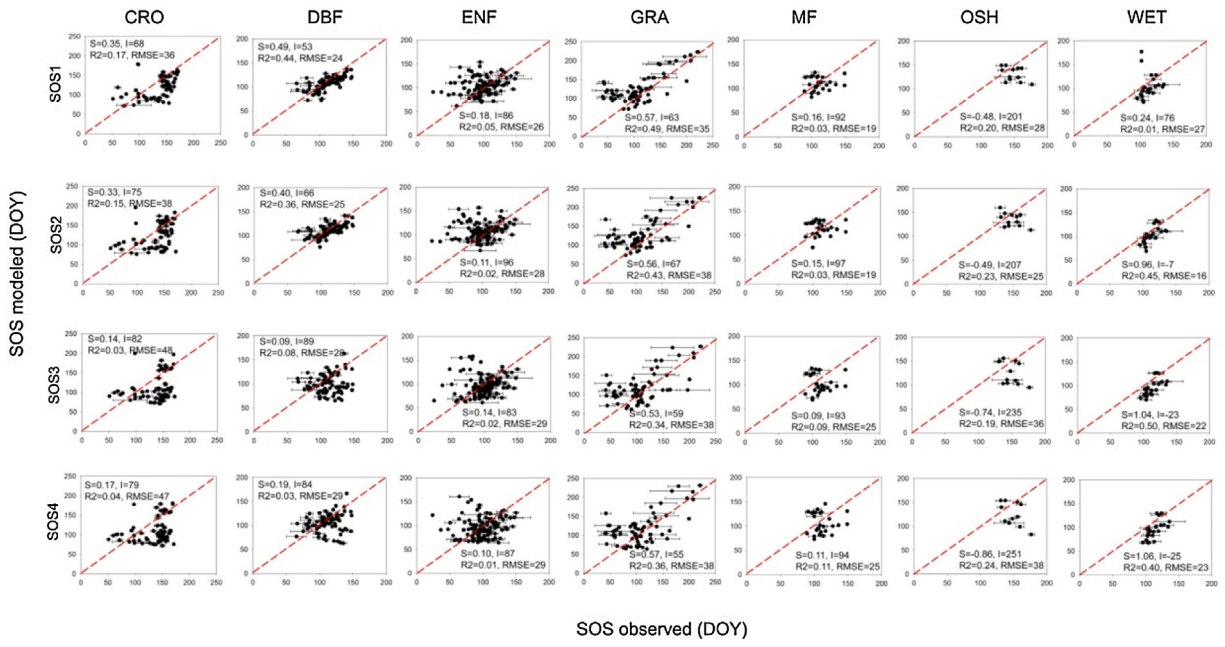

Fig. 10. Relationships between SPOT-VGT modeled start of growing season (SOS) and flux-based observations across plant functional types. SOS1, SOS2, SOS3 and SOS4 are model results for each data fitting approaches (see Method). CRO, DBF, ENF, GRA, MF, OSH and WET represent crop, deciduous broadleaf forest, evergreen needleleaf forest, grassland, mixed forest, open shrub and wetland sites, respectively. Error bar indicates the standard deviation of two flux-based observations. S and I are slope and intercept of regression. Dash line indicates 1:1.

decreased to 20 ± 4.8 and 2.1 ± 4.7 days for SPOT-VGT estimates. For ENF and GRA sites, both MODIS and SPOT-VGT modeled SOS were later than observations, differing in delayed length. Overall, different sensors did not affect the trends when comparing satellite estimated SOS with observations for plant functional types, which was not found for EOS that a more complicated pattern was observed. For example, for MF sites MODIS estimates were earlier than observed EOS while EOS from SPOT-VGT was slightly delayed.

4. Discussion

4.1. Impacts of SOS/EOS extracting methods

Detecting canopy phenology from time series of satellite data using appropriate algorithms is a critical step for applying remotely sensed phenological observations to modeling and scaling efforts (Zhang et al., 2003; Chen et al., 2004; Garrity et al., 2011; Atkinson

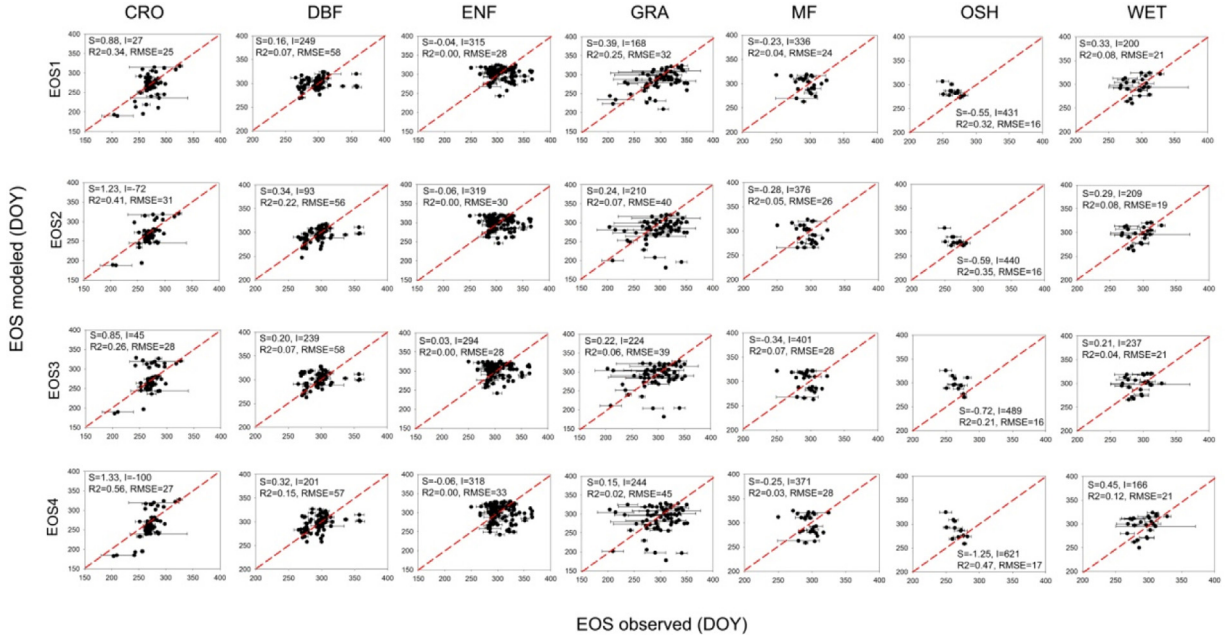

Fig. 11. Relationships between SPOT-VGT modeled end of growing season (EOS) and flux-based observations across plant functional types. EOS1, EOS2, EOS3 and EOS4 are model results for each data fitting approaches (see Method). CRO, DBF, ENF, GRA, MF, OSH and WET represent crop, deciduous broadleaf forest, evergreen needleleaf forest, grassland, mixed forest, open shrub and wetland sites, respectively. Error bar indicates the standard deviation of two flux-based observations. S and I are slope and intercept of regression. Dash line indicates 1:1.

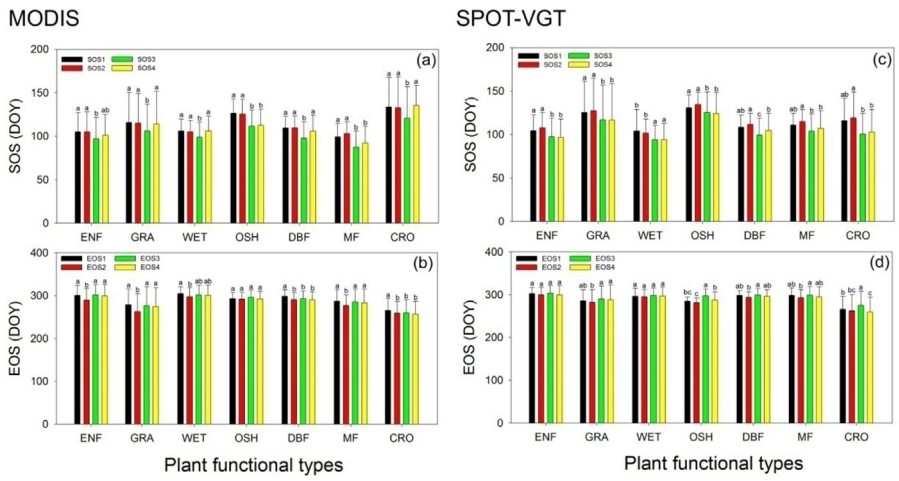

Fig. 12. Comparison between the MODIS (a, b) and SPOT-VGT (c, d) modeled start and end (SOS and EOS) of growing season across plant functional types. EOS1, EOS2, EOS3 and EOS4 are modeled results for each data fitting approaches (see Method). CRO, DBF, ENF, GRA, MF, OSH and WET represent crop, deciduous broadleaf forest, evergreen needleleaf forest, grassland, mixed forest, open shrub and wetland sites, respectively. Error bar indicates the standard deviation for each variable. Lower case shows significant difference from ANOVA analysis within each plant functional type at a significance level of 0.05 (the difference is significant if there is no similar letter).

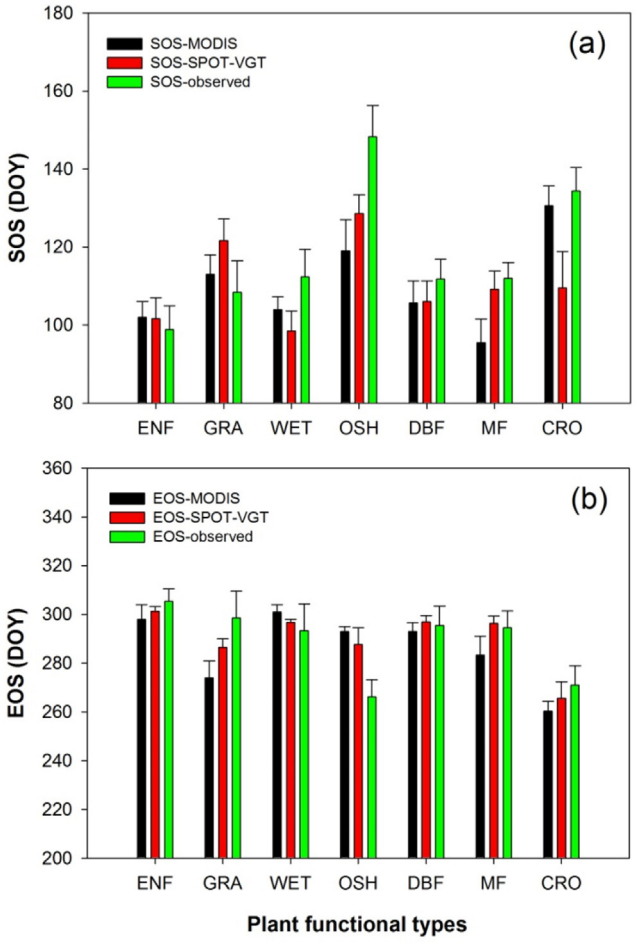

Fig. 13. Comparison between the MODIS and SPOT-VGT modeled (a) start and (b) end (SOS and EOS) of growing season across plant functional types. CRO, DBF, ENF, GRA, MF, OSH and WET represent crop, deciduous broadleaf forest, evergreen needleleaf forest, grassland, mixed forest, open shrub and wetland sites, respectively. Error bar indicates the standard deviation of observations (i.e., different methods) and from different methods within each plant functional types across sites.

et al., 2012; Gonsamo et al., 2012; Kandasamy and Fernandes, 2015; Cao et al., 2015). The typical evolution of contemporary SOS and EOS extraction methods has become more complicated with inclusion of additional variables that are supposed to better interpret plant growth dynamics (e.g., in response to summer decrease in canopy greenness). However, we found that more complex algorithms may not be able to produce better estimates of either SOS or EOS as expected, at least at a coarse spatial scale encompassing several sites. For example, in our analysis SOS from the simple logistic method was much better correlated with observed SOS compared with both double logistic and the more generalized double logistic algorithms (Figs. 4, 6 and 8), though this better performance is less evident for EOS (Fig. 6 and 9). Adding more variables increases the computational burden, but regrettably, higher accuracy may not always be warranted. One reason for such a finding could be that more complicated approaches may indeed better reconstruct the "whole" growth curve at individual sites (e.g., it can better simulate the summer decrease in GPP), but as a cost, the accuracies at the curve maximum increase and decrease in regions where SOS and EOS are expected to happen may decline. Therefore, phenological transitions in spring and autumn may not necessarily be better modeled than that of simple data fitting approaches since the complicated approaches try to reproduce the overall curve, i.e., do not focus on spring and autumn periods. Another limitation of more complicated algorithms is the potential for over-fitting of growth curves so that they are unrealistically sensitive to variations, resulting in false inflection points, and should be carefully removed by post-processing decision. This makes it challenging for them to be applied at regional to continental scales. This is particularly true because there are still sharp waves in the NDVI time-series after applying mSG filter for cropland sites and the drought affected sites under Mediterranean climates and each wave will generate two extremes in the first derivative of the fitted equations, which may be potentially misidentified as the SOS or EOS. It should be stated that the relatively low precision of all predictive methods does not mean that NDVI is not useful for the estimation of phenology, but emphasis on the concern of different responses of algorithms to different plant functional types. The other possible reason for such low correlation may be the time lag, as described in Nagai et al. (2010b), between time-series of NDVI and GPP since they each represent the leaf biomass (i.e., the potential photosynthetic capacity) and the actual photosynthetic activity. Muraoka et al. (2012) also observed

this gap so that for the modeling of SOS/EOS, caution should be given to this issue to improve the estimation accuracy.

4.2. Impacts of different sensors on SOS and EOS

The impacts of different sensors on SOS/EOS modeling were complicated and varied. It seems that all methods driven by MODIS data can simulate SOS slightly better or comparable than those of SPOT-VGT but MODIS data was noticeably less successful for EOS (Fig. 4 vs. Fig. 6 and Fig. 5 vs. Fig. 7, both R^2 and slopes of regression). However, it is worth noting that this difference also was influenced by plant functional type. Apart from sensor design, the most evident difference between these two sensors is the temporal resolution, where MODIS data was acquired for 16 day composite but it was for 10 day composite for SPOT-VGT. One possible reason to explain the performances between SOS and EOS could be that increased frequency of data acquisition may be more prone to noise (e.g., snow melt, spring frost) since NDVI always undergo an accelerated increase in spring. However, in autumn NDVI decreases gradually and high temporal sampling can better reflect the decline in growth. Consequently, there is not much difference in modeling SOS between MODIS and SPOT-VGT while using SPOT-VGT can slight better simulate EOS from NDVI curves. For averaged SOS and EOS from different sensors at the plant functional type perspective, the overall trends are consistent that both MODIS and SPOT-VGT estimates are always larger/lower than observations (Fig. 11). In particular, standard deviation of SOS and EOS explained well the difference between model estimates and observations, irrespective of sensors (Fig. 12). Furthermore, different sensors may also lead to a different significance level of the phenology estimates (Fig. 10), which might worth investigation in future.

4.3. Impacts of plant functional types

Plant functional types clearly impact the performances of NDVI in tracking SOS and EOS. Compared with previous evaluations of NDVI with limited ground observations, our results may have important implications for the usefulness and limitations in NDVI derived from different satellite sensors in predicting SOS and EOS for various plant functional types. NDVI may be the most extensively used vegetation index for phenological studies (Luo et al., 2013), yet has substantially different potentials for the estimation of phenological transitions across biomes. Overall, the variability of canopy greenness may have played the most fundamental role in determining the capability of NDVI for SOS and EOS modeling, which is the same for NDVI from both sensors and from different fitting approaches. For ENF and MF sites, time series of NDVI may have limited strength in reflecting their seasonal dynamics, and consequently, we did not find significant correlation between modeled SOS or EOS (for all fitting methods) and observations. For ecosystems that have much larger seasonal variations in canopy greenness, we observed improved accuracy of modeled SOS and EOS so that different fitting methods may produce estimates that agree well with ground observations (e.g., GRA, DBF and CRO sites in Figs. 8 and 9). These results are consistent with previous evaluations on NDVI for phenological modeling (Soudani et al., 2012; Gonsamo et al., 2012; Hmimina et al., 2013; Xin et al., 2015; D'Odorico et al., 2015; Kandasamy and Fernandes, 2015). The low correlation between modeled SOS/EOS and observations may also be caused by the complicated interactions between changing climate conditions and phenology (Broich et al., 2014; Forkel et al., 2015; Shen et al., 2015; Wu et al., 2016). Of particular importance, our results on the significant difference of outputs (Fig. 10) highlight that cautions should be paid to previous reports on the long-term regional SOS/EOS trends derived from satellite images if the results are not rigorously validated against ground observations.

4.4. Comparison between SOS and EOS

SOS and EOS are important phenological transitions for both annual GPP (Richardson et al., 2010) and NEP (Wu et al., 2012). While there are debates on the important roles each plays in regulating interannual variability of plant productivity (Dragoni et al., 2011; Pilegaard et al., 2011; Wu et al., 2013), it seems that remote sensing of EOS is more challenging, probably because plants often undergo a longer and slower change in canopy greenness in autumn (Richardson et al., 2013; Liu et al., 2016). This difference may lead to a lower interannual variability of changes in EOS relative to SOS, and consequently makes it more difficult to detect it with high accuracy from remote sensing. We also observed this difference in our study that SOS is better modeled than for EOS, irrespective of sensors or plant functional types (Figs. 4–7). The other important aspect to consider is that changes in greenness and NDVI might result from either or changes in LAI and/or chlorophyll contents (Croft et al., 2015). While in spring the rapid development of LAI might result in a good fit for modeled SOS, combined changes in leaf chemistry and LAI might complicate the detection of EOS during senescence. This is in line with results of Nagai et al. (2014) in which several factors (e.g., species, topography) contribute to the high uncertainty of autumn leaf coloring. Our study showed that approaches based on NDVI time series may have limit predictive strength in modeling EOS, highlighting the urgent need to combine other variables (e.g., temperature, water) for a better understanding between phenology and climate change (Gonsamo et al., 2012; Xin et al., 2015; Broich et al., 2014; Liu et al., 2016).

5. Conclusions

Remote sensing of SOS/EOS using satellite observations is challenging, but it remains an essential tool for investigating the impact of climate change on vegetation growth at regional or global scales. Here we tested the potential of both MODIS and SPOT-VGT NDVI derived SOS and EOS at 60 flux sites encompassing seven plant functional types. Overall, we found that NDVI derived phenology had low correlation ($R^2 < 0.30$) with observations, especially for evergreen forests and mixed forests. Care should be given when applying NDVI for SOS and EOS modeling across large scales. Different fitting approaches may produce significantly different estimates of SOS and EOS, with sensor differences also accounting for differences in the fidelity of remotely sensed and observed phenology. Our results highlight the limitation of current SOS/EOS models in reproducing phenological transitions from flux observations, suggesting the importance of applying appropriate algorithms for phenological modeling with respect to both plant functional types and sensors, as well as pointing to the need for rigorous validation of phenology modeling against ground data before its regional applications. Further, they highlight that, given present modeling approaches and sensors, substantial room for improvement exists for using remote sensing applications to predict ecosystem phenology at broad spatial scales. Different combinations of sensor and fitting method may need to be applied for different plant functional types and in particular, identifying these specific best settings to each ecosystem type will be a future research challenge.

Acknowledgements

This work used data from FLUXNET sites and we appreciate the flux PIs providing these valuable data and helpful explanations. This

work was funded by National Natural Science Foundation of China (41371013, 41522109), the key Research Program of Frontier Sciences, CAS to C. Wu (QYZDB-SSW-DQC011), and the International Postdoctoral Funding to A. Gonsamo (Grant No. 2015PE030).

Appendix A. Supplementary data

Supplementary data associated with this article can be found, in the online version, at http://dx.doi.org/10.1016/j.agrformet.2016.11.193.

References

Atkinson, P.M., Jeganathan, C., Dash, J., Atzberger, C., 2012. Inter-comparison of four models for smoothing satellite sensor time-series data to estimate vegetation phenology. Remote Sens. Environ. 123, 400–417.

Baldocchi, D.D., Falge, E., Gu, L.H., Olson, R., Hollinger, D., Running, S., et al., 2001. FLUXNET: a new tool to study the temporal and spatial variability of ecosystem scale carbon dioxide, water vapor, and energy flux densities. Bull. Amer. Meteorol. Soc. 82, 2415–2434.

Broich, M., Huete, A., Tulbure, M.G., Ma, X., Xin, Q., Paget, M., et al., 2014. Land surface phenological response to decadal climate variability across Australia using satellite remote sensing. Biogeosciences 11, 5181–5198.

Cao, R., Chen, J., Shen, M., Tang, Y., 2015. An improved logistic method for detecting spring vegetation phenology in grasslands from MODIS EVI time-series data. Agric. For. Meteorol. 200, 9–20.

Chen, J., Jönsson, P., Tamura, M., Gu, Z., Matsushita, B., Eklundh, L., 2004. A simple method for reconstructing a high-quality NDVI time-series data set based on the Savitzky–Golay filter. Remote Sens. Environ. 91, 332–344.

Christian, B., Joshi, N., Saini, M., Mehta, N., Goroshi, S., Nidamanuri, R.R., et al., 2015. Seasonal variations in phenology and productivity of a tropical dry deciduous forest from MODIS and Hyperion. Agric. For. Meteorol. 214, 91–105.

Croft, H., Chen, J.M., Froelich, N.J., Chen, B., Staebler, R.M., 2015. Seasonal controls of canopy chlorophyll content on forest carbon uptake: implications for GPP modeling. J. Geophys. Res.: Biogeosci. 120, 1576–1586.

D'Odorico, P., Gonsamo, A., Gough, C.M., Bohrer, G., Morison, J., Wilkinson, M., et al., 2015. The match and mismatch between photosynthesis and land surface phenology of deciduous forests. Agric. For. Meteorol. 214, 25–38.

Dash, J., Jeganathan, C., Atkinson, P.M., 2010. The use of MERIS Terrestrial Chlorophyll Index to study spatio-temporal variation in vegetation phenology over India. Remote Sens. Environ. 114, 1388–1402.

de Beurs, K.M., Henebry, G.M., 2004. Land surface phenology, climatic variation, and institutional change: analyzing agricultural land cover change in Kazakhstan. Remote Sens. Environ. 89, 497–509.

Delbart, N., Beaubien, E., Kergoat, L., Le Toan, T., 2015. Comparing land surface phenology with leafing and flowering observations from the PlantWatch citizen network. Remote Sens. Environ. 160, 273–280.

Dragoni, D., Rahman, A.F., 2012. Trends in fall phenology across the deciduous forests of the Eastern USA. Agric. For. Meteorol. 157, 96–105.

Dragoni, D., Schmid, H.P., Wayson, C.A., Potters, H., Grimmond, C.S.B., Randolph, J.C., 2011. Evidence of increased net ecosystem productivity associated with a longer vegetated season in a deciduous forest in south-central Indiana, USA. Global Change Biol. 17, 886–897.

Elmore, A.J., Guinn, S.M., Minsley, B.J., Richardson, A.D., 2012. Landscape controls on the timing of spring, fall, and growing season length in mid-Atlantic forests. Global Change Biol. 18, 656–674.

Fisher, J.I., Mustard, J.F., 2007. Cross-scalar satellite phenology from ground, Landsat, and MODIS data. Remote Sens. Environ. 109, 261–273.

Forkel, M., Migliavacca, M., Thonicke, K., Reichstein, M., Schaphoff, S., Weber, U., Carvalhais, N., 2015. Co-dominant water control on global inter-annual variability and trends in land surface phenology and greenness. Global Change Biol. 21, 3414–3435.

Friedl, M.A., Henebry, G., Reed, B., et al., 2006. Land Surface Phenology: a Community White Paper Request by NASA. ftp://ftp.iluci.org./Land_ESDR/Phenology_Friedl_Whitepaper.pdf.

Friedl, M.A., Sulla-Menashe, D., Tan, B., Schneider, A., Ramankutty, A., Sibley, A., Huang, X., 2010. MODIS Collection 5 global land cover: algorithm refinements and characterization of new datasets. Remote Sens. Environ. 114, 168–182.

Fu, Y.H., Piao, S., Zhao, H., Jeong, S.J., Wang, X., Vitasse, Y., et al., 2014. Unexpected role of winter precipitation in determining heat requirement for spring vegetation green-up at northern middle and high latitudes. Global Change Biol. 20, 3743–3755.

Fu, Y.H., Zhao, H., Piao, S., Peaucelle, M., Peng, S., Zhou, G., et al., 2015. Declining global warming effects on the phenology of spring leaf unfolding. Nature 526, 104–107.

Garrity, S.R., Maurer, K.D., Mueller, K.L., Vogel, C.S., Curtis, P.S., 2011. A comparison of multiple phenology data sources for estimating seasonal transitions in deciduous forest carbon exchange. Agric. For. Meteorol. 151, 1741–1752.

Gonsamo, A., Chen, J.M., Price, D.T., Kurz, W.A., Wu, C., 2012. Land surface phenology from optical satellite measurement and CO_2 eddy covariance technique. J. Geophys. Res. 117, http://dx.doi.org/10.1029/2012JG002070.

Hmimina, G., Dufrene, E., Pontailler, J.Y., Delpierre, N., Aubinet, M., Caquet, B., et al., 2013. Evaluation of the potential of MODIS satellite data to predict vegetation phenology in different biomes: an investigation using ground-based NDVI measurements. Remote Sens. Environ. 132, 145–158.

Huete, A., Didan, K., Miura, T., Rodriguez, E.P., Gao, X., Ferreira, L.G., 2002. Overview of the radiometric and biophysical performance of the MODIS vegetation indices. Remote Sens. Environ. 83, 195–213.

Hufkens, K., Friedl, M., Sonnentag, O., Braswell, B.H., Milliman, T., Richardson, A.D., 2012. Linking near-surface and satellite remote sensing measurements of deciduous broadleaf forest phenology. Remote Sens. Environ. 117, 307–321.

Jeganathan, C., Dash, J., Atkinson, P.M., 2014. Remotely sensed trends in the phenology of northern high latitude terrestrial vegetation, controlling for land cover change and vegetation type. Remote Sens. Environ. 143, 154–170.

Jenkins, J.P., Braswell, B.H., Frolking, S.E., Aber, J.D., 2002. Detecting and predicting spatial and interannual patterns of temperate forest springtime penology in the eastern U.S. Geophys. Res. Lett. 29, 2201, http://dx.doi.org/10.1029/2001GL014008.

Jeong, S.J., Ho, C.H., Gim, H.J., Brown, M.E., 2011. Phenology shifts at start vs: end of growing season in temperate vegetation over the Northern Hemisphere for the period 1982–2008. Glob. Change Biol 17, 2385–2399.

Kandasamy, S., Fernandes, R., 2015. An approach for evaluating the impact of gaps and measurement errors on satellite land surface phenology algorithms: application to 20 year NOAA AVHRR data over Canada. Remote Sens. Environ. 164, 114–129.

Keenan, T.F., Darby, B., Felts, E., Sonnentag, O., Friedl, M.A., Hufkens, K., et al., 2014a. Tracking forest phenology and seasonal physiology using digital repeat photography: a critical assessment. Ecol. Appl. 24, 1478–1489.

Keenan, T.F., Gray, J., Friedl, M.A., Toomey, M., Bohrer, G., Hollinger, D.Y., et al., 2014b. Net carbon uptake has increased through warming-induced changes in temperate forest phenology. Nat. Climate Change 4, 598–604.

Klosterman, S., Hufkens, K., Gray, J.M., Melaas, E., Sonnentag, O., Lavine, I., et al., 2014. Evaluating remote sensing of deciduous forest phenology at multiple spatial scales using PhenoCam imagery. Biogeosciences 11, 4305–4320.

Kogan, F.N., 1997. Global drought watch from space. Bull. Am. Meteorol. Soc. 78, 621–636.

Liu, Y., Wu, C., Peng, D., Xu, S., Gonsamo, A., Jassal, R.S., Arain, M.A., Lu, L., Fang, B., Chen, J.M., 2016. Improved modeling of land surface phenology using MODIS land surface reflectance and temperature at evergreen needleleaf forests of central North America. Remote Sens. Environ. 176, 152–162.

Luo, X., Chen, X., Xu, L., Myneni, R., Zhu, Z., 2013. Assessing performance of NDVI and NDVI3 g in monitoring leaf unfolding dates of the deciduous broadleaf forest in Northern China. Remote Sens. 5, 845–861.

Maisongrande, P., Duchemin, B., Dedieu, G., 2004. VEGETATION/SPOT: an operational mission for the Earth monitoring; presentation of new standard products. Int. J. Remote Sens. 25, 9–14.

Melaas, E.K., Friedl, M.A., Zhu, Z., 2013. Detecting interannual variation in deciduous broadleaf forest phenology using Landsat TM/ETM+ data. Remote Sens. Environ. 132, 176–185.

Melaas, E.K., Friedl, M.A., Richardson, A.D., 2016. Multi-scale modeling of spring phenology across Deciduous Forests in the Eastern United States. Glob. Change Biol. 22, 792–805, http://dx.doi.org/10.1111/gcb.13122.

Morisette, J.T., Richardson, A.D., Knapp, A.K., Fisher, J.I., Graham, E.A., Abatzoglou, J., Wilson, B.E., Breshears, D.D., Henebry, G.M., Hanes, J.M., Liang, L., 2009. Tracking the rhythm of the seasons in the face of global change: phenological research in the 21 st century. Front. Ecol. Environ. 7, 253–260.

Motohka, T., Nasahara, K.N., Oguma, H., Tsuchida, S., 2010. Applicability of green-red vegetation index for remote sensing of vegetation phenology. Remote Sens. 2, 2369–2387.

Muraoka, H., Noda, H.M., Nagai, S., Motohka, T., Saitoh, T.M., Nasahara, K.N., et al., 2012. Spectral vegetation indices as the indicator of canopy photosynthetic productivity in a deciduous broadleaf forest. J. Plant Ecol. 6, 393–407.

Nagai, S., Nasahara, K.N., Muraoka, H., Akiyama, T., Tsuchida, S., 2010a. Field experiments to test the use of the normalized-difference vegetation index for phenology detection. Agric. For. Meteorol. 150, 152–160.

Nagai, S., Saigusa, N., Muraoka, H., Nasahara, K.N., 2010b. What makes the satellite-based evi–gpp relationship unclear in a deciduous broad-leaved forest? Ecol. Res. 25, 359–365.

Nagai, S., Inoue, T., Ohtsuka, T., Kobayashi, H., Kurumado, K., Muraoka, H., et al., 2014. Relationship between spatio-temporal characteristics of leaf-fall phenology and seasonal variations in near surface- and satellite-observed vegetation indices in a cool-temperate deciduous broad-leaved forest in Japan. Int. J. Remote Sens. 35, 3520–3536.

Papale, D., Valentini, A., 2003. A new assessment of European forests carbon exchange by eddy fluxes and artificial neural network spatialization. Global Change Biol. 9, 525–535.

Park, H., Jeong, S.J., Ho, C.H., Kim, J., Brown, M.E., Schaepman, M.E., 2015. Nonlinear response of vegetation green-up to local temperature variations in temperate and boreal forests in the Northern Hemisphere. Remote Sens. Environ. 165, 100–108.

Peichl, M., Sonnentag, O., Nilsson, M.B., 2015. Bringing color into the picture: using digital repeat photography to investigate phenology controls of the carbon dioxide exchange in a boreal mire. Ecosystems 18, 115–131.

Piao, S., Fang, J., Zhou, L., Ciais, P., Zhu, B., 2006. Variations in satellite-derived phenology in China's temperate vegetation. Glob. Change Biol. 12, 672–685.

Piao, S., Wang, X., Ciais, P., Zhu, B., Wang, T., Liu, J., 2011. Changes in satellite-derived vegetation growth trend in temperate and boreal Eurasia from 1982 to 2006. Global Change Biol. 17, 3228–3239.
Piao, S., Tan, J., Chen, A., Fu, Y.H., Ciais, P., Liu, Q., et al., 2015. Leaf onset in the northern hemisphere triggered by daytime temperature. Nat. Commun. 6, http://dx.doi.org/10.1038/ncomms7911.
Pilegaard, K., Ibrom, A., Courtney, M.S., Hummelshøj, P., Jensen, N.O., 2011. Increasing net CO_2 uptake by a Danish beech forest during the period from 1996 to 2009. Agric. For. Meteorol. 151, 934–946.
Reichstein, M., Falge, E., Baldocchi, D., Papale, D., Aubinet, M., Berbigier, P., et al., 2005. On the separation of net ecosystem exchange into assimilation and ecosystem respiration: review and improved algorithm. Global Change Biol. 11, 1424–1439.
Richardson, A.D., Black, T.A., Ciais, P., Delbart, N., Friedl, M.A., Gobron, N., et al., 2010. Influence of spring and autumn phenological transitions on forest ecosystem productivity. Philos. Trans. R. Soc. London B Biol. Sci. 365, 3227–3246.
Richardson, A.D., Anderson, R.S., Arain, M.A., et al., 2012. Terrestrial biosphere models need better representation of vegetation phenology: results from the North American Carbon Program Site Synthesis. Global Change Biol. 18, 566–584.
Richardson, A.D., Keenan, T.F., Migliavacca, M., Ryu, Y., Sonnentag, O., Toomey, M., 2013. Climate change, phenology, and phenological control of vegetation feedbacks to the climate system. Agric. For. Meteorol. 169, 156–173.
Rodriguez-Galiano, V.F., Dash, J., Atkinson, P.M., 2015. Inter-comparison of satellite sensor land surface phenology and ground phenology in Europe. Geophys. Res. Lett. 42, 2253–2260.
Rouse, J.W., Haas, R.H., Schell, J.A., Deering, D.W., Harlan, J.C., 1974. Monitoring the vernal advancements and retrogradation of natural vegetation. In: NASA/GSFC, Final Report. Greenbelt, MD, USA, pp. 1–137.
Ryu, Y., Lee, G., Jeon, S., Song, Y., Kimm, H., 2014. Monitoring multi-layer canopy spring phenology of temperate deciduous and evergreen forests using low-cost spectral sensors. Remote Sens. Environ. 149, 227–238.
Shen, M., Piao, S., Cong, N., Zhang, G., Jassens, I.A., 2015. Precipitation impacts on vegetation spring phenology on the Tibetan Plateau. Global Change Biol. 21, 3647–3656.
Sonnentag, O., Hufkens, K., Teshera-Sterne, C., Young, A.M., Friedl, M., Braswell, B.H., et al., 2012. Digital repeat photography for phenological research in forest ecosystems. Agric. For. Meteorol. 152, 159–177.
Soudani, K., Hmimina, G., Delpierre, N., Pontailler, J.Y., Aubinet, M., Bonal, D., Caquet, B., de Grandcourt, A., Burban, B., Flechard, C., Guyon, D., Granier, A., Gross, P., Heinesh, B., Longdoz, B., Loustau, D., Moureaux, C., Ourcival, J.M., Rambal, S., Saint André, L., Dufrêne, E., et al., 2012. Ground-based Network of NDVI measurements for tracking temporal dynamics of canopy structure and vegetation phenology in different biomes. Remote Sens. Environ. 123, 234–245.
Verma, M., Friedl, M.A., Law, B.E., Bonal, D., Kiely, G., Black, T.A., et al., 2015. Improving the performance of remote sensing models for capturing intra-and inter-annual variations in daily GPP: An analysis using global FLUXNET tower data. Agric. For. Meteorol. 214, 416–429.
Walker, J.J., De Beurs, K.M., Wynne, R.H., Gao, F., 2012. Evaluation of Landsat and MODIS data fusion products for analysis of dryland forest phenology. Remote Sens. Environ. 117, 381–393.
White, M.A., Nemani, R.R., 2006. Real-time monitoring and short-term forecasting of land surface phenology. Remote Sens. Environ. 104, 43–49.
White, M.A., Beurs, D., Kirsten, M., Didan, K., Inoue, D.W., Richardson, A.D., et al., 2009. Intercomparison, interpretation, and assessment of spring phenology in North America estimated from remote sensing for 1982–2006. Global Change Biol. 15, 2335–2359.
Wu, C., Chen, J.M., Desai, A.R., Hollinger, D.Y., Arain, M.A., Margolis, H.A., et al., 2012. Remote sensing of canopy light use efficiency in temperate and boreal forests of North America using MODIS imagery. Remote Sens. Environ. 118, 60–72.
Wu, C., Chen, J.M., Black, T.A., Price, D.T., Kurz, W.A., Desai, A.R., et al., 2013. Interannual variability of net ecosystem productivity in forests is explained by carbon flux phenology in autumn. Global Ecol. Biogeogr. 22, 994–1006.
Wu, C., Gonsamo, A., Gough, C.M., Chen, J.M., Xu, S., 2014. Modeling growing season phenology in North American forests using seasonal mean vegetation indices from MODIS. Remote Sens. Environ. 147, 79–88.
Wu, C., Hou, X., Peng, D., Gonsamo, A., Xu, S., 2016. Land surface phenology of China's temperate ecosystems over 1999–2013: Spatial–temporal patterns, interaction effects, covariation with climate and implications for productivity. Agric. For. Meteorol. 216, 177–187.
Xin, Q., Broich, M., Zhu, P., Gong, P., 2015. Modeling grassland spring onset across the Western United States using climate variables and MODIS-derived phenology metrics. Remote Sens. Environ. 161, 63–77.
Xu, L., Saatchi, S.S., Yang, Y., Myneni, R.B., Frankenberg, C., Chowdhury, D., Bi, J., 2015. Satellite observation of tropical forest seasonality: spatial patterns of carbon exchange in Amazonia. Environ. Res. Lett. 10, 084005.
Zhang, X., Goldberg, M.D., 2011. Monitoring fall foliage coloration dynamics using time-series satellite data. Remote Sens. Environ. 115, 382–391.
Zhang, X., Friedl, M.A., Schaaf, C.B., Strahler, A.H., Hodges, J.C.F., Gao, F., et al., 2003. Monitoring vegetation phenology using MODIS. Remote Sens. Environ. 84, 471–475.
Zhang, X., Tan, B., Yu, Y., 2014. Interannual variations and trends in global land surface phenology derived from enhanced vegetation index during 1982–2010. Int. J. Bioclimatol. 58, 547–564.
Zhang, X., 2015. Reconstruction of a complete global time series of daily vegetation index trajectory from long-term AVHRR data. Remote Sens. Environ. 156, 457–472.